

Prediction of fluid velocity slip at solid surfaces

J. S. Hansen*

DNRF Centre “Glass and Time”, IMFUFA, Department of Sciences, Roskilde University, P.O. Box 260, DK-4000 Roskilde, Denmark

B. D. Todd†

Faculty of Engineering & Industrial Sciences and Centre for Molecular Simulation, Swinburne University of Technology, P.O. Box 218, Hawthorn, Victoria 3122, Australia

Peter J. Daivis‡

School of Applied Sciences, RMIT University, G.P.O. Box 2476, Melbourne, Victoria 3001, Australia

(Received 14 February 2011; published 25 July 2011)

The observed flow enhancement in highly confining geometries is believed to be caused by fluid velocity slip at the solid wall surface. Here we present a simple and highly accurate method to predict this slip using equilibrium molecular dynamics. Unlike previous equilibrium molecular dynamics methods, it allows us to directly compute the intrinsic wall-fluid friction coefficient rather than an empirical friction coefficient that includes all sources of friction for planar shear flow. The slip length predicted by our method is in excellent agreement with the slip length obtained from direct nonequilibrium molecular dynamics simulations.

DOI: [10.1103/PhysRevE.84.016313](https://doi.org/10.1103/PhysRevE.84.016313)

PACS number(s): 47.15.Cb, 62.25.-g, 47.11.Mn

I. INTRODUCTION

For a complete continuum dynamical description of the flow of a confined fluid, one needs to specify the boundary conditions. Traditionally, a no-slip or slip Dirichlet boundary condition is applied, where the fluid velocity at the wall must be known *a priori*. More generally the boundary condition is formulated in terms of the slip length, L_s , and the shear rate at the interface, i.e., via a Neumann boundary condition. There have been numerous studies of the slip phenomenon [1–11], starting from Navier [12] in 1823 (see Karniadakis *et al.* [13] for an overview), but only a few of these studies have considered the derivation of correlation function expressions for the slip length. The first solutions to this problem were presented by Bocquet and Barrat [5], who presented two methods for computing the slip length from equilibrium correlation functions. Their first method uses a fit to the correlation function of the transverse momentum density to obtain the two slip lengths at the upper and lower walls and the width of the channel as fitting parameters. The fluid viscosity, which is also required, is obtained from separate simulations performed on a homogeneous fluid at the same temperature and density as the bulk fluid phase in the center of the channel. This method gave excellent results, but it is rather complicated to implement and does not seem to have been widely adopted. In addition, this method assumes macroscopic hydrodynamic behavior across the whole system, including a constant value of the viscosity, which, for very narrow channels, may not be justified. The second method presented in Bocquet and Barrat’s paper relates the wall friction coefficient to the integral of the autocorrelation function of the wall-fluid force. The final expression is similar to a Green-Kubo relation, but Bocquet and Barrat remarked that it did not produce results in

quantitative agreement with the method based on the transverse momentum density autocorrelation function.

The force autocorrelation function method was recently discussed by Petravic and Harrowell [9,10], who found that the friction coefficient computed in the force autocorrelation function method is actually the total fluid friction for shear flow in the confined fluid, including the slip friction at both interfaces as well as the viscous friction in the fluid. This is clearly seen by the following argument. Consider planar shear flow between two walls. If slip flow occurs at either or both of the walls, the total velocity difference between the two planar walls is $\Delta u = \Delta u_1 + \Delta u_L + \Delta u_2$, where Δu_1 and Δu_2 are the slip velocities at the two walls and Δu_L is the velocity difference across the shearing fluid. In mechanical equilibrium, the shear stress is constant across the whole system. At each wall, the stress is given by a constitutive equation of the form $P_{yx} = -\xi_1 \Delta u_1$ and in the shearing fluid we can apply Newton’s law of viscosity, $P_{yx} = -\eta \Delta u_L / L_y$. We can also introduce an effective friction coefficient μ representing the combined effect of all sources of friction by defining $P_{yx} = -\mu \Delta u$. Substituting these constitutive equations into the equation for the sum of the velocity differences, we find $1/\mu = 1/\xi_1 + 1/\xi_2 + L_y/\eta$. This simple equation, which is analogous to the equation for the effective resistance of resistors in parallel, was derived by Petravic and Harrowell. Examining the constitutive equation defining the friction coefficient obtained from the integral of the force autocorrelation function by Bocquet and Barrat [5] [see their Eq. (4.13)], we see that their expression actually defines the effective friction rather than the slip friction coefficient. A similar point was made by Bhatia and Nicholson [14] in relation to the friction coefficient calculated from the fluid center-of-mass velocity autocorrelation function. In certain limiting cases, the slip friction should make a dominant contribution to the effective friction, i.e., when the channel width L_y approaches zero or when the slip friction coefficients approach zero, leading to plug flow, as is often found for the flow of water next to a

*jschmidt@ruc.dk

†btodd@swin.edu.au

‡peter.daivis@rmit.edu.au

hydrophobic wall. In such cases, the effective friction should give a good estimate of the slip friction, but in cases where this limiting behavior is not observed, it is necessary to remove the viscous contribution to the total friction in order to compute the slip friction coefficient and, even then, it is only the combined effect of the friction at both walls that is obtained. Note that the effective friction is also system size dependent, since the viscous friction term contains the channel width, L_y . A more direct method of computing the slip friction coefficient is clearly needed.

In this paper we follow Navier’s original work and derive an expression for the center-of-mass velocity of a thin fluid layer adjacent to one wall. This expression is only dependent on the intrinsic wall-fluid friction coefficient, which can be found via equilibrium (nondriven) molecular dynamics simulations. Using the expression for the center-of-mass velocity of the fluid layer and the value of the friction coefficient, the slip length can be predicted. We compare the predictions with direct nonequilibrium molecular dynamics (NEMD) simulation data showing excellent agreement. Our method, therefore, provides a convenient way to predict the slip at a fluid-solid interface without needing to extract the slip friction from an effective friction coefficient.

The paper is organized as follows: In the next section we briefly discuss the Navier slip boundary condition and present our treatment that leads to a slip length based on an intrinsic friction coefficient. In Sec. III we summarize the simulation details and describe how to calculate the friction coefficient from equilibrium molecular dynamics (EMD) simulations. Section IV presents the results, comparing the predicted slip length with direct NEMD simulations. Section V shows the applicability of our method to the case where a fluid is confined between two different walls and undergoes a planar Hagen-Poiseuille flow. In the last section we summarize the conclusions.

II. THEORY

A. The Navier boundary condition

Consider a fluid with velocity field $\mathbf{u} = (u, v, w)$ flowing over a surface S . The surface may possess a velocity \mathbf{u}_w . Using the fluid velocity as a reference, we define the relative velocity as $\delta\mathbf{u} \equiv (\delta u, \delta v, \delta w) = \mathbf{u}_w - \mathbf{u}$. Now, let S be normal to the y direction and $\mathbf{n} = (0, 1, 0)$. If the Reynolds number is sufficiently low the flow is laminar (or unidirectional), say, in the x direction. The Navier boundary condition can then be written as [15]

$$\delta u - \frac{\sigma_{xy}}{\zeta_N} = 0 \text{ on } S, \quad (1)$$

where σ_{xy} is the xy stress tensor component. Applying Newton’s law of viscosity, which relates the shear stress with the strain rate $\dot{\gamma}$ as $\sigma_{xy} = \eta_0 \dot{\gamma}$, Eq. (1) yields

$$\frac{\eta_0}{\zeta_N} \dot{\gamma} = L_s \left. \frac{\partial u}{\partial y} \right|_{y=y_w} = \delta u, \quad (2)$$

where η_0 is the shear viscosity. In Eq. (2) y_w is the y coordinate of S and L_s is the slip length given by $L_s = \eta_0/\zeta_N$. Note that Eq. (2) is simply a Neumann boundary condition. The slip length can also be interpreted as the value of y where the

tangent line $t(y) = \partial u/\partial y|_{y=y_w} y - \delta u$ is zero, and L_s may therefore take a negative value depending on the geometry. To avoid this ambiguity we write the magnitude of the slip length as

$$|L_s| = \eta_0/\zeta_N. \quad (3)$$

The Navier friction coefficient is a material property which depends on the wall-fluid interactions. Bocquet and Barrat [5] proposed a Green-Kubo-type integral for ζ_N . However, it was later shown [9] that their integral depends on system size; i.e., the coefficient was not a material parameter that quantifies the wall-fluid friction alone. As mentioned in the introduction, slip has been studied extensively over the years; however, it still remains to develop a satisfactory method to evaluate the intrinsic wall-fluid friction.

B. The wall-fluid friction

Analogous to the above discussion, assume that a fluid is confined between two parallel walls with positions $y_w = 0$ (wall 1) and $y_w = L_y$ (wall 2), respectively. This means that the y direction is the direction of confinement. We consider a fluid element with constant mass, m , and average volume $V = L_x \Delta L_z$, that is, a fluid slab adjacent to wall 1 and of average width Δ . See Fig. 1. The fluid may be subjected to an external constant force per unit mass F_e in the x direction. The acceleration of the slab in this direction is governed by Newton’s second law, i.e.,

$$m \frac{du_{\text{slab}}}{dt} = F'_x(t) + F''_x(t) + mF_e, \quad (4)$$

where u_{slab} is the center-of-mass velocity of the slab (adjacent to wall 1) in the x direction, F'_x is the force due to wall-slab interactions, and F''_x is the force due to fluid-slab interactions. The microscopic definition of the slab center of mass is given in Eq. (36). Note that F''_x includes a kinetic contribution due to the momentum of fluid particles entering and leaving the slab. Furthermore, it should be mentioned that the fluid-fluid forces between particles inside the slab cancel out due to Newton’s third law and do not contribute to the slab acceleration.

The wall-slab force term, F'_x , can be viewed as a frictional shear force that depends on the relative velocity between the

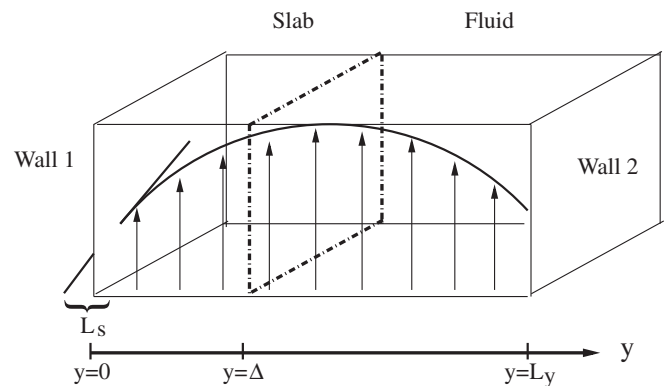


FIG. 1. Schematic illustration of the system. The arrows inside the box indicate the velocity field forming the profile. L_s is the slip length and Δ is the slab width, typically an order of magnitude smaller than system width L_y .

wall and the fluid. For sufficiently small relative velocities, we may propose the following linear constitutive equation relating the wall-slab shear force to the velocity difference, $\Delta u' = u_{\text{slab}} - u_w$:

$$F'_x(t) = - \int_0^t \zeta(t - \tau) \Delta u'(\tau) d\tau + F'_r(t), \quad (5)$$

where ζ is a friction kernel. F'_r is a random force term with zero mean that is assumed to be uncorrelated with u_{slab} ; that is,

$$\langle F'_r(t) \rangle = 0 \quad \text{and} \quad \langle u_{\text{slab}}(0) F'_r(t) \rangle = 0. \quad (6)$$

For steady flows the time average of Eq. (5) is given by

$$\langle F'_x \rangle = -\zeta_0 \langle \Delta u' \rangle, \quad (7)$$

where ζ_0 is the zero frequency friction coefficient. It is worth noting that Eq. (5) defines a true slip friction coefficient; i.e., the kernel ζ only depends on the velocity difference between the wall and an adjacent fluid layer and therefore overcomes the system size dependencies of other methods.

In order to account for the fluid-slab shear force, F''_x , one can apply Newton's law of viscosity. Thus, for steady flows we have

$$\langle F''_x \rangle = A \eta_0 \langle \dot{\gamma} \rangle = A \eta_0 \left. \frac{\partial u}{\partial y} \right|_{y=\Delta}, \quad (8)$$

where $A = L_x L_z$ is the surface area.

The slab width, Δ , is a critical parameter. If it is chosen to be much smaller than the width of the first fluid layer adjacent to the wall, the center-of-mass velocity of the slab will be a poor approximation to the velocity at a certain slip plane [16] due to the extremely small number of molecules inside the slab. On the other hand, for large values of Δ , the center-of-mass velocity of the slab will be an average that includes a substantial contribution from fluid that is far from the wall. In this case, the difference between the center-of-mass slab velocity and the wall velocity is not equal to the slip plane velocity and it would not be correct to use the center-of-mass slab velocity in the constitutive equation defining the intrinsic slip friction coefficient, Eq. (5). Ultimately, the optimal slab width must be a compromise between a value that is large enough to completely include the layer of fluid that slips over the surface and one that is small enough to exclude fluid that experiences normal shear flow, i.e., a purely viscous flow. This optimal value is expected to depend on the details of the intermolecular interactions as well as the thermodynamic state of the system.

C. Derivation of the slip length

In the remainder of the paper we focus on steady flows. Since the slab has finite width we use integral boundary conditions (IBCs) which enable us solve the Navier-Stokes equations in terms of u_{slab} rather than the fluid velocity at some slip plane. In this way we also obtain an equation for the strain rate at $y = \Delta$. From Eq. (4) we can then express u_{slab} as a function of the friction coefficient ζ_0 using Eqs. (7) and (8). This finally leads to an explicit equation for the slip length using Eq. (2).

In general, the IBCs read

$$\bar{u}^{(1)} = \frac{1}{\Delta} \int_0^\Delta u(y) dy \quad \text{and} \quad \bar{u}^{(2)} = \frac{1}{\Delta} \int_{L_y-\Delta}^{L_y} u(y) dy. \quad (9)$$

Thus, it is the same as the center-of-mass velocity of a slab under the assumption that the fluid density is constant. For example, for the lower boundary we have

$$\begin{aligned} u_{\text{c.m.}} &= \frac{1}{m} \int_V \rho u(y) dV = \frac{L_x L_z \rho}{m} \int_0^\Delta u(y) dy \\ &= \frac{1}{\Delta} \int_0^\Delta u(y) dy, \end{aligned} \quad (10)$$

where we recall that $V = L_x \Delta L_z$ and $\rho = m/V$. Thus, if wall 1 is at rest, the average center-of-mass velocity of the slab, $\langle u_{\text{slab}} \rangle$, can be approximated with $\bar{u}^{(1)}$.

For a Couette flow with identical walls and where wall 2 has velocity u_w the Navier-Stokes equation reduces to a simple Laplace equation

$$\frac{\partial^2 u}{\partial y^2} = 0 \quad (11)$$

with IBCs

$$\begin{aligned} \bar{u}^{(1)} &= \langle u_{\text{slab}} \rangle = \frac{1}{\Delta} \int_0^\Delta u(y) dy \quad \text{and} \\ \bar{u}^{(2)} &= u_w - \langle u_{\text{slab}} \rangle = \frac{1}{\Delta} \int_{L_y-\Delta}^{L_y} u(y) dy, \end{aligned} \quad (12)$$

which yields the solution

$$u = \frac{u_w - 2\langle u_{\text{slab}} \rangle}{L_y - \Delta} \left(y - \frac{\Delta}{2} \right) + \langle u_{\text{slab}} \rangle. \quad (13)$$

Notice that in the solution, Eq. (13), there are no boundary value conditions for $y = 0$ or $y = L_y$ as in the classical approach: the profile is now determined by the slab center-of-mass velocity as given by the IBC. The strain rate at $y = \Delta$ is then

$$\dot{\gamma} = \frac{u_w - 2\langle u_{\text{slab}} \rangle}{L_y - \Delta}. \quad (14)$$

For a Couette flow, Eq. (4) reads $\langle F'_x \rangle + \langle F''_x \rangle = 0$; that is, from Eqs. (7), (8), and (14),

$$-\zeta_0 \langle u_{\text{slab}} \rangle + A \eta_0 \frac{u_w - 2\langle u_{\text{slab}} \rangle}{L_y - \Delta} = 0, \quad (15)$$

which is rearranged to give an expression for the average slab center-of-mass velocity at wall 1, namely,

$$\langle u_{\text{slab}} \rangle = \frac{\eta_0 u_w}{\xi_0 (L_y - \Delta) + 2\eta_0}, \quad (16)$$

where $\xi_0 = \zeta_0/A$. The slip length now follows from Eq. (2), by substituting Eq. (16) into Eq. (13); thus, for wall 1 we have

$$L_s = -u(0) \left. \frac{\partial u}{\partial y} \right|_{y=0}^{-1} = \frac{\Delta}{2} - \frac{\eta_0}{\xi_0}. \quad (17)$$

Note that $L_s < 0$ due to our geometry as discussed above. In the limit of zero slab width, $\Delta \rightarrow 0$, we obtain

$$|L_s| = \eta_0 / \xi_0 \quad (18)$$

in accordance with the Navier slip length, Eq. (3). We note here that there exists a clear definition of the friction coefficient $\xi_0 = \zeta_0/A$ [see Eq. (5)]; i.e., it is possible to measure this quantity directly (see Sec. III).

If an external force per unit mass, F_e , is applied to the fluid and both walls are at rest, the Navier-Stokes equation is reduced to the Stokes (or Poisson) equation

$$\frac{\partial^2 u}{\partial y^2} = -\frac{\rho F_e}{\eta_0} \quad (19)$$

subject to the IBCs

$$\begin{aligned} \bar{u}^{(1)} &= \langle u_{\text{slab}} \rangle = \frac{1}{\Delta} \int_0^\Delta u(y) dy \quad \text{and} \\ \bar{u}^{(2)} &= \langle u_{\text{slab}} \rangle = \frac{1}{\Delta} \int_{L_y-\Delta}^{L_y} u(y) dy. \end{aligned} \quad (20)$$

The solution to this boundary value problem is

$$u = \frac{\rho F_e}{12\eta_0} [6y(L_y - y) + \Delta(2\Delta - 3L_y)] + \langle u_{\text{slab}} \rangle, \quad (21)$$

which resembles a planar Hagen-Poiseuille flow. For this steady flow Newton's second law is $\langle F'_x \rangle + \langle F''_x \rangle + mF_e = 0$. Applying the constitutive equations (7) and (8) we obtain

$$-\zeta_0 \langle u_{\text{slab}} \rangle + \frac{A\rho F_e}{2}(L_y - 2\Delta) + mF_e = 0, \quad (22)$$

giving

$$\langle u_{\text{slab}} \rangle = \frac{\rho F_e L_y}{2\xi_0} \quad (23)$$

by assuming constant density. Note that since $\langle u_{\text{slab}} \rangle$ increases with increasing slab width, it can be seen from Eq. (23) that ξ_0 must be a decreasing function of Δ , that is, if the density is constant. The slip length follows as

$$L_s = \Delta \left(\frac{1}{2} - \frac{\Delta}{3L_y} \right) - \frac{\eta_0}{\xi_0}, \quad (24)$$

which means that $|L_s| = \eta_0/\xi_0$ as $\Delta \rightarrow 0$ as expected. It is important to note here that the slip length given in Eq. (24) is different from Eq. (17) with the term $-\Delta^2/3L_y$; that is, the slip length depends on the flow type for nonzero slab width. In principle, this contradicts the findings of Cieplak *et al.* [17] and we comment on this later.

III. MOLECULAR DYNAMICS

A. Calculating the friction coefficient

For $u_w = 0$, Eq. (5) is written as

$$F'_x(t) = -\int_0^t \zeta(t-\tau) u_{\text{slab}}(\tau) d\tau + F'_r(t). \quad (25)$$

Multiplying both sides with $u_{\text{slab}}(0)$ and taking the ensemble average it is possible to form the corresponding relation between the slab velocity-force correlation function $C_{uF'_x}$ and the slab velocity autocorrelation function C_{uu} ,

$$C_{uF'_x}(t) = -\int_0^t \zeta(t-\tau) C_{uu}(\tau) d\tau, \quad (26)$$

such that

$$C_{uF'_x}(t) = \langle u_{\text{slab}}(0) F'_x(t) \rangle \quad \text{and} \quad C_{uu}(t) = \langle u_{\text{slab}}(0) u_{\text{slab}}(t) \rangle. \quad (27)$$

In Eq. (27) we used the properties of F'_r as given in Eq. (6). We can transform Eq. (26) into a more convenient algebraic form by a Laplace transform yielding

$$\tilde{C}_{uF'_x}(s) = -\tilde{\zeta}(s) \tilde{C}_{uu}(s), \quad (28)$$

where the Laplace transformation is defined as

$$\mathcal{L}[f(t)] = \int_0^\infty f(t) e^{-st} dt = \tilde{f}(s). \quad (29)$$

We assume that the friction kernel can be written as an n -term Maxwellian memory function [18]

$$\zeta(t) = \sum_{i=1}^n B_i e^{-\lambda_i t}, \quad (30)$$

which means that

$$\tilde{\zeta}(s) = \sum_{i=1}^n \frac{B_i}{s + \lambda_i}. \quad (31)$$

Substituting this into Eq. (28), we trivially get

$$\tilde{C}_{uF'_x}(s) = -\sum_{i=1}^n \frac{B_i \tilde{C}_{uu}(s)}{s + \lambda_i}. \quad (32)$$

We here focus on steady flows, as we are primarily interested in ζ_0 . From Eq. (30) we have

$$\zeta_0 = \int_0^\infty \sum_{i=1}^n B e^{-\lambda_i t} dt = \sum_{i=1}^n B_i / \lambda_i. \quad (33)$$

It is important to point out that the friction can be evaluated directly from Eq. (28), that is, without suggesting a functional form of the kernel. However, we find that this gives rather large statistical errors, especially for large s . Using EMD simulations it is possible to evaluate $C_{uF'_x}$ and C_{uu} and therefore also the Laplace transforms. From this, one can fit the right-hand side of Eq. (32) to the $\tilde{C}_{uF'_x}$ data using B_i and λ_i as fitting parameters.

B. Simulation details

The molecular dynamics simulations are carried out using standard techniques [19,20]. All particles (fluid molecules and wall atoms) are simple spherical particles that interact via a truncated and shifted Lennard-Jones-type potential

$$\phi_{\text{tr}}(r_{ij}) = \begin{cases} 4\epsilon \left[\left(\frac{\sigma}{r_{ij}} \right)^{12} - \left(\frac{\sigma}{r_{ij}} \right)^6 \right] - \phi(r_c) & \text{if } r_{ij} \leq r_c, \\ 0 & \text{if } r_{ij} > r_c, \end{cases} \quad (34)$$

where r_{ij} is the distance between particles i and j , ϵ and σ are the interaction strength and the length scale, respectively, and ϕ is the untruncated potential. We have calculated ζ_0 for different wall-fluid interaction potentials, which we denote ϕ_{wf} : one is purely repulsive (relatively hydrophobic) by setting $r_c = 2^{1/6}\sigma$ (the Weeks-Chandler-Andersen (WCA) potential [21]). The other is the classical Lennard-Jones (LJ) potential with $r_c = 2.5\sigma$ that possesses both a repulsive and attractive part [19] and is relatively hydrophilic. We have also changed the fluid-fluid

TABLE I. Listing of the different systems. ϕ_{wf} and ϕ_{ff} denote the wall-fluid interaction and fluid-fluid interaction potentials, respectively. WCA is an abbreviation for the Weeks-Chandler-Andersen potential and LJ is the Lennard-Jones potential. The values for the shear viscosities, η_0 , are interpolated from Rowley and Painter [22] and Hansen *et al.* [23]

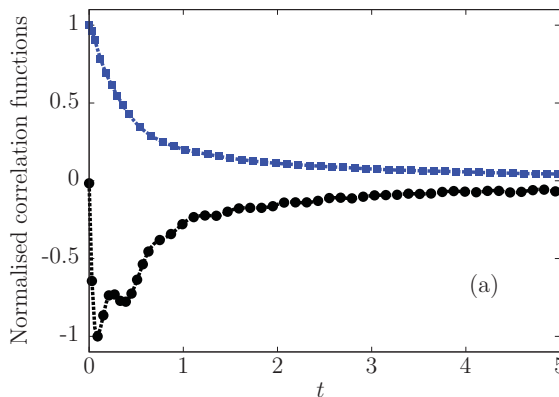
System	ϕ_{wf}	ϕ_{ff}	ρ_{bulk}	ρ_{wall}	Temperature	η_0
1	WCA	WCA	0.51	0.80	0.80	0.43
2	LJ	WCA	0.44	0.80	0.80	0.31
3	LJ	LJ	0.79	0.90	0.73	1.94
4	WCA	WCA	0.70	0.80	0.73	1.03

interaction potential, ϕ_{ff} , between the WCA and LJ potentials. One can express any mechanical quantity in units of σ , ϵ , and particle mass m_i . Thus, the temperature, T , is written as $T^* = k_B T / \epsilon$, number density as $\rho^* = \rho \sigma^3$, time as $t^* = t / (\sigma \sqrt{m_i / \epsilon})$, and so forth. In the remainder of the paper we use these dimensionless units and omit the asterisk. Table I lists the different systems, where we note that all quantities are given in standard dimensionless molecular dynamics (MD) units.

The wall particles are initially arranged on a face-centered cubic lattice and kept around their initial (or equilibrium) positions \mathbf{r}_{eq} via a restoring spring potential: $\phi_s = \frac{1}{2} k_s (\mathbf{r}_i - \mathbf{r}_{\text{eq}})^2$, where $k_s = 150$ is the spring constant and \mathbf{r}_i is the position of the wall particle. A wall is composed of three wall particle layers and by applying periodic boundary conditions one single wall acts as a first and second wall. The wall temperature is kept around a certain temperature by using a Nosé-Hoover scheme [24,25] which thermostats the fluid to that temperature as well. The equations of motion for all particles were integrated forward in time using a leap-frog integration scheme [26] with time step $\Delta t = 0.001$. Unless otherwise stated the system's dimensions are $L_x = L_z = 10.36$ and $L_y = 13.47$, giving the area $A = 107.27$.

During the simulations the wall-slab shearing force is evaluated directly via

$$F'_x(t) = \sum_{\substack{i \in \text{slab} \\ j \in \text{wall}}} F_{ij,x}(t), \quad (35)$$



where $F_{ij,x}$ is the force in the x direction on slab particle i due to wall particle j at time t . The x component of the center-of-mass velocity of the slab was calculated via

$$u_{\text{slab}}(t) = \frac{1}{m} \sum_{i \in \text{slab}} m_i v_{i,x}(t), \quad (36)$$

where $v_{i,x}$ is the velocity of slab particle i and $m = \sum_{i \in \text{slab}} m_i$. From these quantities it is possible to evaluate the correlation functions $C_{uF'_x}$ and C_{uu} . The correlation times are dependent on the slab width, Δ , and in order to ensure convergence the correlation functions are sampled over a time span of 200–300 time units. We stress again that since the number of particles in the slab is constant, which is accomplished by allowing the slab width to undergo small fluctuations, Δ is an average value over time.

C. Verification with direct NEMD simulations

To verify the theory we carried out a series of direct NEMD simulations. To this end we applied either an external force field to generate a planar Hagen-Poiseuille flow or added an additional wall and moved it with a certain speed u_w in the x direction to simulate a Couette flow. The streaming velocity profiles were obtained using a bin method; see, for example, Hansen *et al.* [27]. We stress that the strain rate is maintained sufficiently low to avoid any significant viscous heating of the fluid; i.e., the heat conduction at the thermostated walls is able to keep the temperature of the fluid constant. Furthermore, the low strain rate also ensures the existence of a laminar flow due to the low Reynolds number.

From the direct NEMD simulations we can calculate the slip length. This involves taking the numerical derivative of the velocity profile which is associated with very large statistical uncertainties. To overcome this problem we fitted the velocity profile to either a first- or second-order polynomial depending on the flow type and extracted the tangent line at $y = 0$ (and thereby the slip length) from this fit.

IV. RESULTS AND DISCUSSION

Figure 2(a) shows an example of the correlation functions $C_{uF'_x}$ and C_{uu} for $\Delta \approx 1$ and for short times. It is observed that

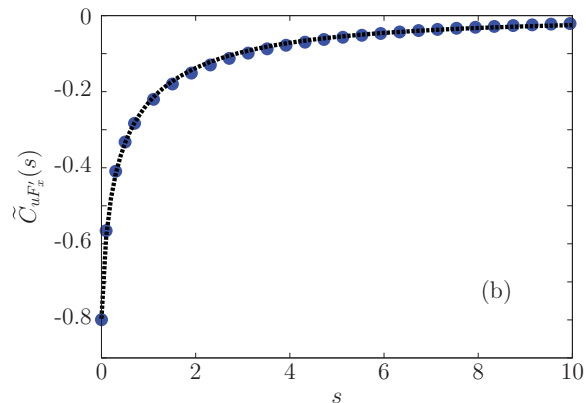


FIG. 2. (Color online) (a) Section of the normalized correlation functions $C_{uF'_x}$ (points connected with lines) and C_{uu} (squares connected with lines) vs time. The functions are normalized with respect to their maximum absolute value. This example is for system 3 and $\Delta \approx 1$. (b) Corresponding Laplace transformation of $C_{uF'_x}$ (points) together with the best fit of Eq. (32) to the data using a one-term Maxwellian memory function (dashed line). $B_1 = 353$ and $\lambda_1 = 4.80$.

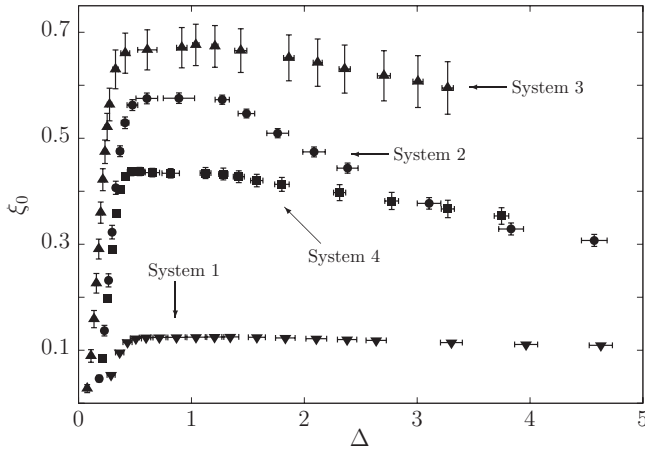


FIG. 3. ξ_0 as a function of slab width Δ for system 1 (downward pointing triangles), system 2 (circles), system 3 (upward pointing triangles), and system 4 (squares). Error bars show the standard error.

the slab velocity and slab force are anticorrelated which is due to the fact that the shear force acts in the opposite direction to the slab velocity. In order to suppress high-frequency noise at the end of each correlation data set we applied a Hann window [28] before the Laplace transformation which was carried out using a simple trapezoidal integration scheme. Figure 2(b) depicts the corresponding Laplace transform of the slab force-velocity correlation function (points) together with the best fit of Eq. (32) using $n = 1$. We also tried to fit the simulation data with other functional forms; however, the Maxwellian memory function fitted the data best. It is seen that a one-term Maxwellian memory function is sufficient to describe the relation between C_{uF_x} and C_{uu} . In fact, this is true for all the systems studied here. From Eq. (33) we obtain a friction coefficient: $\xi_0 = \zeta_0/A = B_1/(A\lambda_1) \approx 0.69$.

As discussed in Sec. II B, the friction coefficient is dependent on the slab width, Δ . Figure 3 shows ξ_0 as a function of slab width for the four different systems studied here. First, it is observed that the friction is low when the wall-fluid interaction is purely repulsive, yielding a large slip as expected. Second, it can be seen that the friction coefficient

varies dramatically for small slab widths as one would expect since more of the wall-fluid interactions are included as Δ increases. From Δ around 0.75 to 1.25 the friction coefficient features a maximum before decreasing. For larger slab widths the dominating wall-fluid interactions are included; however, in this regime the friction coefficient is no longer an intrinsic property of the wall-fluid friction, since it includes both frictional and viscous forces. We do therefore not expect, or intend, the theory to hold for large Δ . It is important to stress, however, that the fact that ξ_0 decreases is not an indication that the theory breaks down *per se*: in fact, from Eq. (23) we would expect the friction coefficient to decrease. In order to study the effect of the slab width further we compared the predicted slab velocities, Eqs. (16) and (23), with direct NEMD simulations of a Couette flow and planar Hagen-Poiseuille flow (see Fig. 4). For the Couette flow, Fig. 4(a), the predicted slab velocity is in excellent agreement with the simulation data for $0.75 < \Delta < 2.25$ as expected from the discussion above. This is also found for the Hagen-Poiseuille flow. We can only expect the theory to be valid for sufficiently small strain rates, or for small values of the external force in the case for the Hagen-Poiseuille flow. This is highlighted in Fig. 4(b) where it is shown that the theory cannot predict the slab velocity correctly for large F_e . We note that the maximum strain rate in Fig. 4(a) is around 0.03, which is smaller than the two largest strain rates in Fig. 4(b) corresponding to $F_e = 0.0075$ and $F_e = 0.01$.

In order to follow Navier’s original idea, one can extrapolate the friction coefficient to $\Delta = 0$. However, no unique extrapolation gives the correct values of the slab velocity. This indicates that the frictional shear force is indeed dependent on the slab width in a highly nontrivial manner. Since we cannot extrapolate the friction coefficient to zero slab width we cannot predict the velocity exactly at the wall (i.e., for $y = 0$). Thus, the calculated slip corresponds to the apparent slip [15]. From these findings we conjecture that there exists an interfacial region where the theory is valid. This region stretches from the wall and one or two particle diameters into the fluid for van der Waals-type interactions.

As mentioned in the introduction, alternative methods are based on coefficients that are system size dependent

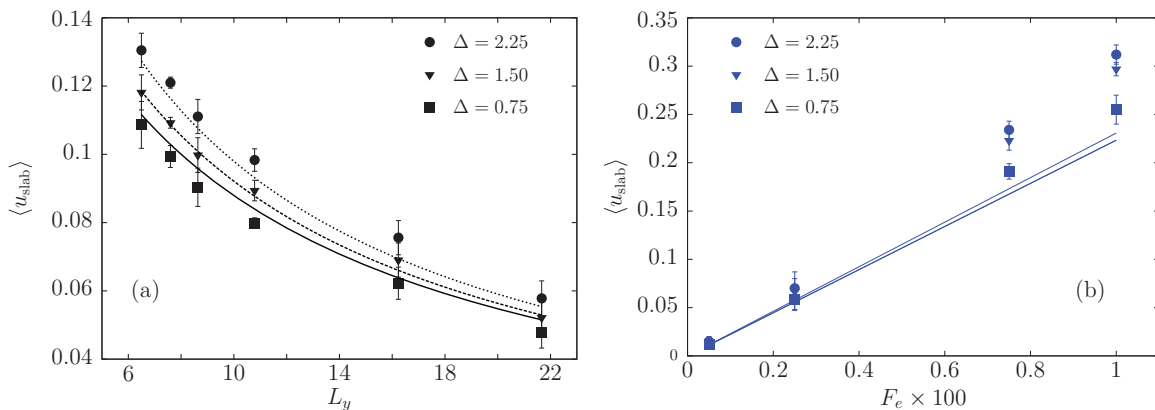


FIG. 4. (Color online) (a) Average slab velocity as a function of L_y for different slab widths in the case of a Couette flow. Symbols are from direct NEMD simulations and lines represent the predictions from Eq. (16). (b) Average slab velocity as a function of F_e for different slab widths in the case of a Hagen-Poiseuille flow. Symbols are from direct NEMD simulations and lines represent the predictions from Eq. (23). Both (a) and (b) show results for system 1 (see Table I).

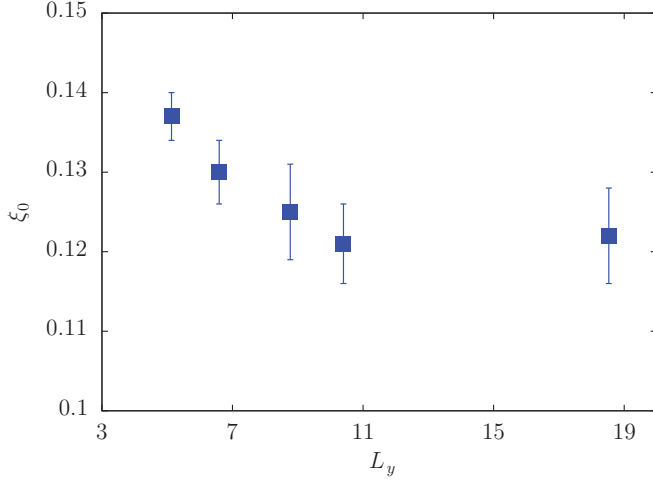


FIG. 5. (Color online) ξ_0 as a function of channel width for system 1 where $\Delta \approx 1.2$.

[9,14]. Since the theory presented in this paper is based on the dynamics of a single fluid slab rather than the entire system, we argued that ζ is system size independent. To check this, we calculated ξ_0 for $\Delta \approx 1.2$ for different channel widths: the result is summarized in Fig. 5. It is seen that for sufficiently wide channel widths ($L_y \gtrsim 7$) the friction coefficient is indeed constant. Very small channel widths ($L_y \lesssim 7$) are characterized by spatial correlation effects that influence the fluid transport properties [20,27,29,30]; thus, the constitutive relation, Eq. (5), fails and the kernel should include a convolution in space as well.

In Fig. 6 we plotted the slip lengths obtained from direct NEMD simulations of Hagen-Poiseuille and Couette flows versus the predicted slip length for all four systems and for sufficiently low strain rates. It is clearly seen that the predictions given by Eqs. (17) and (24) are in excellent agreement with the NEMD simulation data. Recall that our

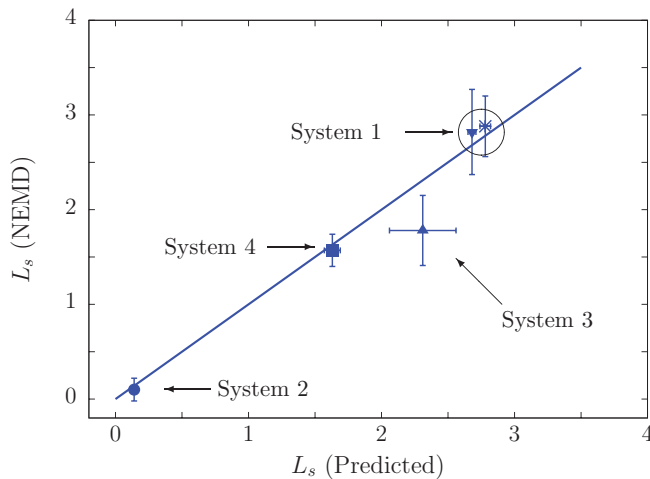


FIG. 6. (Color online) Slip length obtained from direct NEMD simulations vs predicted slip lengths for planar Hagen-Poiseuille flows with $L_y = 7.7$ (circle, square, and triangles) and Couette flow with $L_y = 21.8$ (cross). $\Delta \approx 1.5\sigma$. Results for all four systems are shown. Error bars show the standard error and the straight line indicates perfect agreement.

predictions of the slip lengths indicate that it is dependent on the flow type. This contradicts the finding by Cieplak *et al.* [17], which is based on direct NEMD simulations. For system 1 we evaluated the slip length for both a Couette and a Hagen-Poiseuille flow where L_y is 21.8 and 7.7, respectively. For the Hagen-Poiseuille flow, this is around the lowest channel width that we can apply before the classical hydrodynamical theory breaks down [20] and where ξ_0 is system size independent (see Fig. 5): it is therefore the maximum effect we can obtain from the additional $-\Delta^2/(3L_y)$ term in Eq. (24). It is seen that since L_y is typically orders of magnitude larger than the interfacial region, Δ , the effect from the term cannot be measured using direct NEMD within statistical error. We can further quantify the effect via the relative difference in the slip length between a Couette and a Hagen-Poiseuille flow, which is given by

$$\Delta L_s^{\text{rel}} = \frac{2\Delta^2\xi_0}{3L_y(\Delta\xi_0 - 2\eta_0)}, \quad L_y > 0. \quad (37)$$

In Fig. 6, system 1, this corresponds to a 1.8% difference which cannot be measured in NEMD simulations.

V. APPLICATION: PLANAR HAGEN-POISEUILLE FLOW WITH DIFFERENT BOUNDARY CONDITIONS

The method presented here provides a very convenient and accurate way to predict the slip for any flow and for any system without having to recalculate the friction coefficient. To illustrate this important point consider a WCA fluid undergoing a planar Hagen-Poiseuille flow with the same geometry as above. Let the fluid interact with wall 1 via the purely repulsive WCA potential and with wall 2 via the LJ

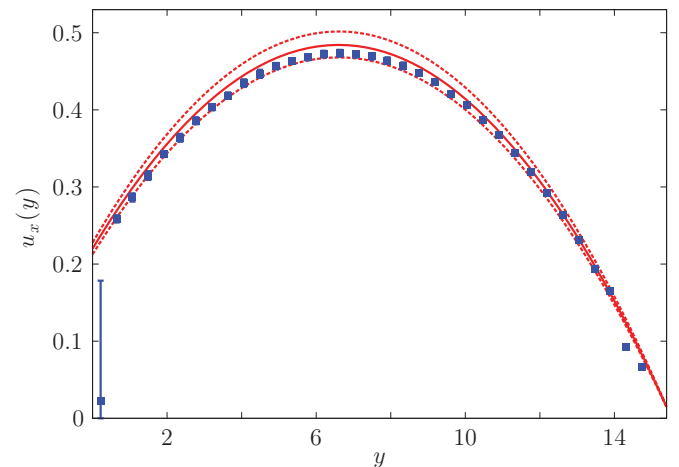


FIG. 7. (Color online) Comparison between the predicted velocity profile (lines) and direct NEMD data (solid squares) for a WCA fluid where left wall-fluid interactions are governed by a WCA (hydrophobic) potential and right are governed by the LJ potential (hydrophilic). Error bars on the NEMD data show the standard error: in the interior of the channel the errors are smaller than the size of the symbols. The two dashed (or dotted) lines represent the profiles obtained using the maximum and minimum shear viscosity that are within standard error, i.e., $\eta_0 = 0.418$ and $\eta_0 = 0.390$ ($\rho \approx 0.49$). The solid line is the profile for the mean value $\eta_0 = 0.404$.

potential. The slip lengths at wall 1 and wall 2 are denoted L'_s and L''_s , respectively. The boundary value problem then reads

$$\frac{\partial^2 u}{\partial y^2} = -\frac{\rho F_e}{\eta_0} \quad (38)$$

with

$$L'_s \left. \frac{\partial u}{\partial y} \right|_{y=0} = -u(0) \quad \text{and} \quad L''_s \left. \frac{\partial u}{\partial y} \right|_{y=L_y} = -u(L_y). \quad (39)$$

This can readily be solved, yielding

$$u(y) = -\frac{\rho F_e}{2\eta_0} [y^2 + A(L'_s - y)], \quad (40)$$

where

$$A = \frac{L_y(L_y - 2L''_s)}{L'_s + L_y - L''_s}. \quad (41)$$

Now applying the slip lengths obtained above for system 1 and system 2 we can predict the velocity profile. Figure 7 depicts the streaming velocity profile given by Eq. (40). Direct NEMD data (squares) of the same system are also plotted in the figure, showing excellent agreement.

VI. CONCLUSION

We have here presented an accurate and versatile method to predict the fluid slip at solid surfaces. The method is based on an intrinsic wall-fluid friction coefficient which can be found from equilibrium MD simulations. Once the friction

coefficient is determined, the slip length follows from Eqs. (17) and (24). This leads to an easy and accurate prediction of the fluid velocity profile. Unlike previous methods, the friction calculated by our method is an intrinsic property of the wall-fluid interactions for a specified wall and it therefore excludes all other sources of friction in the channel. This yields a slip length that can be applied directly in the continuum description of confined fluids.

We stress that using previously suggested methods [5,9–11] one would have to recalculate the system-specific friction coefficient, which makes using these methods cumbersome. In contrast our method allows one to compute the friction coefficient from a single EMD simulation for the particular wall-fluid system. Once this is determined the slip length is easily predicted for any flow. The significance of this is that it obviates the need to perform time intensive NEMD simulations to determine the flow profiles of systems in which slip is important. Instead, one can use Eqs. (17) and (24) (or equivalent for other flow types) and accurately predict the slip and flow profiles in a fraction of the time required to perform NEMD computations.

ACKNOWLEDGMENTS

The authors would like to thank the Australian Research Council for supporting this work as a part of a Discovery grant (Grant No. DP 0663759). Also, we thank Professor Gary Bryant for valuable comments on the manuscript.

-
- [1] J. C. Maxwell, *Philos. Trans. R. Soc. London* **170**, 231 (1879).
 [2] J. Koplik, J. Banavar, and J. Willemsen, *Phys. Fluids A* **1**, 781 (1989).
 [3] F. Brochard and P. G. de Gennes, *Langmuir* **8**, 3033 (1992).
 [4] Z. Guo, T. S. Zhao, and Y. Shi, *Phys. Rev. E* **71**, 035301 (2005).
 [5] L. Bocquet and J.-L. Barrat, *Phys. Rev. E* **49**, 3079 (1994).
 [6] O. Vinogradova, *Langmuir* **11**, 2213 (1995).
 [7] C. J. Mundy, S. Balasubramanian, and M. L. Klein, *J. Chem. Phys.* **105**, 3211 (1996).
 [8] S. Heidenreich, P. Ilg, and S. Hess, *Phys. Rev. E* **75**, 066302 (2007).
 [9] J. Petracic and P. Harrowell, *J. Chem. Phys.* **127**, 174706 (2007).
 [10] J. Petracic and P. Harrowell, *J. Chem. Phys.* **128**, 209901 (2008).
 [11] V. P. Sokhan and N. Quirke, *Phys. Rev. E* **78**, 015301 (2008).
 [12] C. L. M. H. Navier, *Mem. Acad. Sci. Inst. Fr.* **6**, 389 (1823).
 [13] G. Karniadakis, A. Beskok, and N. Aluru, *Microflows and Nanoflows: Fundamentals and Simulation* (Springer, New York, 2005).
 [14] S. K. Bhatia and D. Nicholson, *Phys. Rev. Lett.* **100**, 236103 (2008).
 [15] L. G. Leal, *Advanced Transport Phenomena* (Cambridge University Press, New York, 2007).
 [16] C. Denniston and M. O. Robbins, *J. Chem. Phys.* **125**, 214102 (2006).
 [17] M. Cieplak, J. Koplik, and J. R. Banavar, *Phys. Rev. Lett.* **86**, 803 (2001).
 [18] D. J. Evans and G. P. Morriss, *Statistical Mechanics of Nonequilibrium Liquids* (Academic, New York, 1990).
 [19] M. P. Allen and D. J. Tildesley, *Computer Simulation of Liquids* (Clarendon, New York, 1989).
 [20] K. P. Travis, B. D. Todd, and D. J. Evans, *Phys. Rev. E* **55**, 4288 (1997).
 [21] J. D. Weeks, D. Chandler, and H. C. Andersen, *J. Chem. Phys.* **54**, 5237 (1971).
 [22] R. L. Rowley and M. M. Painter, *Int. J. Thermophys.* **18**, 1109 (1997).
 [23] J. S. Hansen, P. J. Daivis, K. P. Travis, and B. D. Todd, *Phys. Rev. E* **76**, 041121 (2007).
 [24] S. Nosé, *Mol. Phys.* **52**, 255 (1984).
 [25] W. G. Hoover, *Phys. Rev. A* **31**, 1695 (1985).
 [26] D. Frenkel and B. Smit, *Understanding Molecular Simulation* (Academic, London, 1996).
 [27] J. S. Hansen, P. J. Daivis, and B. D. Todd, *J. Chem. Phys.* **126**, 144706 (2007).
 [28] W. Press, W. Vetterling, S. Teukolsky, and B. Flannery, *Numerical Recipes in C* (Cambridge University Press, Cambridge, 1992).
 [29] B. D. Todd, J. S. Hansen, and P. J. Daivis, *Phys. Rev. Lett.* **100**, 195901 (2008).
 [30] B. D. Todd and J. S. Hansen, *Phys. Rev. E* **78**, 051202 (2008).